ACS Catalysis

Research Article

pubs.acs.org/acscatalysis

Surface Oxidation of Stainless Steel: Oxygen Evolution Electrocatalysts with High Catalytic Activity

Helmut Schäfer,*[,†] Seyyed Mohsen Beladi-Mousavi,[†] Lorenz Walder,[†] Joachim Wollschläger,[‡] Olga Kuschel,[‡] Sachar Ichilmann,[†] Shamaila Sadaf,[†] Martin Steinhart,[†] Karsten Küpper,[‡] and Lilli Schneider[‡]

[†]Institute of Chemistry of New Materials and Center of Physics and Chemistry of New Materials and [‡]Fachbereich Physik, Universität Osnabrück, Barbarastrasse 7, 49076 Osnabrück, Germany

Supporting Information

ABSTRACT: The cheap stainless commodity steel AISI 304, which basically consists of Fe, Ni, and Cr, was surface-oxidized by exposure to Cl_2 gas. This treatment turned AISI 304 steel into an efficient electrocatalyst for water splitting at pH 7 and pH 13. The overpotential of the anodic oxygen evolution reaction (OER), which typically limits the efficiency of the overall water-splitting process, could be reduced to 260 mV at 1.5 mA/cm^2 in 0.1 M KOH. At pH 7, overpotentials of 500−550 mV at current densities of 0.65 mA/cm^2 were achieved. These values represent a surprisingly good activity taking into account the simplicity of the procedure and the fact that the starting material is virtually omnipresent. Surface-oxidized AISI 304 steel exhibited outstanding long-term stability of its electrocatalytic properties in the alkaline as well as in the neutral regime, which did not deteriorate even after chronopoteniometry for 150 000 s. XPS analysis revealed that surface oxidation resulted in the formation of Fe oxide and Cr oxide surface layers with a thickness in the range of a few nanometers accompanied by enrichment of Cr in the surface layer. Depending on the duration of the Cl_2 treatment, the purity of the Fe oxide/Cr oxide mixture lies between 95% and 98%. Surface oxidation of AISI 304 steel by chlorination is an easy and scalable access to nontoxic, cheap, stable, and efficient electrocatalysts for water splitting.

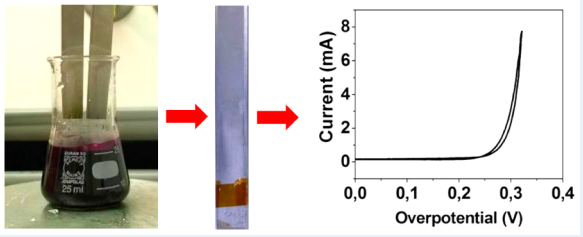

KEYWORDS: *solar to fuel conversion, renewable energy sources, oxygen evolution electrocatalysis, stainless steel, surface oxidation, XPS spectroscopy*

1. INTRODUCTION

Analogous to photosynthesis, solar energy may be captured and artificially stored as chemical energy in solar fuels by exploitation of water splitting, the conversion of water into hydrogen and oxygen.[1−3] Because water is a virtually inexhaustible raw material, hydrogen and oxygen production in water−alkali electrolyzers is highly economical and limitless. Hence, water splitting may pave the way for environmentally friendly, inoffensive production of large amounts of solar fuels as required by a potential hydrogen economy.[4] Hydrogen, with a price of 8 €/kg, is the more valuable water-splitting product. Nevertheless, the oxygen evolution reaction (OER) at the anode is as important as the hydrogen evolution reaction (HER) at the cathode for two reasons. On the one hand, ideal solar fuel for fuel cells consists of both hydrogen and oxygen. On the other hand, the total overpotential of the electrochemical water-splitting process is the sum of the overpotentials at the cathode and the anode. There is a stringent need to optimize the anode process because the majority of the total overpotential of state-of-the-art systems is generated at the anode. As a matter of fact, the OER is the efficiency-limiting step for the overall water-splitting process because of the high OER overpotentials. The OER is a complex process involving the transfer of 4 electrons:

$$4OH^- \rightarrow O_2 + 2H_2O + 4e^-$$

Efficient electrocatalysts for solar-to-fuel conversion must operate close to Nernstian potentials (E), i.e., the applied potential should not strongly differ from the reversible H_2O/O_2 potential (1.228 V vs RHE at 298.15 K) to yield acceptable current densities. Technically feasible current densities range from 5 to >500 mA/cm, depending on the concept[2,5−7] Typically, these requirements are met by noble metal containing catalysts like rutile-type IrO_2 and RuO_2.[8−15] However, the technical use of these catalysts is impeded by their limited availability and by their high costs. Although these oxides have been shown to be rather stable in polymer electrolyte membrane (PEM) cells,[16] they do not exhibit long-term stability under alkaline water electrolysis conditions.[17] Thus, implementation of the production of mixtures of H_2 and O_2 as solar fuels by water splitting has been hampered by a lack

Received: September 30, 2014
Revised: March 16, 2015
Published: March 17, 2015

© 2015 American Chemical Society

DOI: 10.1021/acscatal.5b00221
ACS Catal. 2015, 5, 2671−2680

of efficient, stable and low-priced catalysts consisting of readily available elements.

Pourbaix diagrams allow identifying promising candidates for the optimization of the OER overpotential, including IrO_2 and RuO_2 as well as potential alternatives, revealing again the crucial role of oxides as electrocatalysts for OER. Thus, Hoar showed that even in the case of noble metals, no oxygen is released as long as the corresponding metal oxide is not formed on the catalyst surface.[18,19] To scale up solar fuel production by water splitting, it is highly desirable to use catalytic materials for OER in alkaline medium that consist of cheap, readily available metals. For example, the performance of various MnO_x species with different compositions, morphologies, and structures in the water-splitting process has been investigated but suffers from low electrocatalytic efficiency.[20−23] Mixed spinel oxides such as $NiCo_2O_4$[19,24] and Perovskite-type compounds such as $LaNiO_3$[25] have been intensively studied and optimized with respect to their water-splitting properties, but their synthesis is laborious. To the best of our knowledge, little effort has been devoted to tests of the water-splitting performance of these materials in the neutral regime. More recently, benchmark species such as $Ba_{0.5}Sr_{0.5}Co_{0.8}Fe_{0.2}O_y$[26] with an overpotential of ∼360 mV at 10 mA/cm^2 in 0.1 M KOH, nanocrystalline Ni_3S_2 supported by metallic Ni with an overpotential of 187 mV at 10 mA/cm^2 in 0.1 M KOH,[27] and $CuFe(MoO_4)_3$ with an overpotential of 245 mV at 10 mA/cm^2 in 1 M KOH[28] were developed. Nickel has been commercially used as a catalyst for anodic water splitting[16,29,30] and remains the anode of choice in industrial electrolyzers especially for water splitting in hot alkaline solutions.[2]

Many groups showed that the electrocatalytic OER properties of Ni especially when it is accompanied by iron can be significantly improved. Corrigan et al., for instance, investigated the coprecipitation of Ni and Fe in Ni-based thin films.[31,32]

It is straightforward to assume that commercially available, nontoxic, cheap stainless steels such as AISI 304 steel, AISI 316 steel, and AISI 316L are suitable candidates for water splitting because they contain the earth-abundant elements Fe, Ni, Co, Mn, which are known as active centers in water-splitting electrocatalysts. However, the electrocatalytic performance of steel regarding OER in the alkaline regime is at best mediocre. To the best of our knowledge, the highest catalytic activities reported for steel or iron in electrochemical water splitting in alkaline medium are 360 mV overpotential at 1 mA/cm^2 in 1 M NaOH,[33] 600 mV overpotential at 10 mA/cm^2 in 0.1 M NaOH,[34] and 320 mV overpotential at 10 mA/cm^2 in 1 M KOH.[35] In addition, the suitability of steel as a catalyst for the electrocatalytically initiated water splitting in neutral regime has not been proven up to now.

Here we report a simple modification procedure that renders industrial steel AISI 304 containing the earth-abundant metals Ni and Cr into a water-splitting electrocatalyst that exhibits surprising catalytic activity for OERs in alkaline as well as in neutral media. AISI 304 is a common austenitic grade that is widely used in industry. We show that modification of AISI 304 steel by treatment with gaseous Cl_2 leads to pronounced increase in the concentration of catalytically active Cr and Fe centers and in turn to significantly improved electrocatalytic oxygen evolution properties in alkaline and neutral media. To the best of our knowledge, Cl_2 has so far not been used for surface oxidation of steel in order to improve electrocatalytic properties in the OER. Surface-oxidized AISI 304 steel show not only low overpotentials but also excellent long-term stability of its electrocatalytic properties.

2. EXPERIMENTAL DETAILS

Materials. All samples were prepared from X5CrNi18-10 (304) steel, thereafter referred to as AISI 304 steel, with a thickness of 1.5 mm. The steel was cut in stripes with a length of 100 mm and a width of 10 mm. The surface of the X5CrNi18-10 (304) steel pieces was carefully cleaned with ethanol, polished with grit 600 SiC sanding paper, and rinsed with deionized water.

Surface Oxidation of AISI 304 Steel by Gaseous Chlorine (Samples SO60−SO300). Cl_2 gas was generated right before use by oxidation of aqueous HCl solution with $KMnO_4$ (Figure S1a) in a 25 mL Erlenmeyer flask. One gram (6.3 mmol) of $KMnO_4$ (VWR, Darmstadt) was dissolved under stirring in 15 mL of deionized water. Then, we added 1 mL of a 37 wt % HCl solution (VWR, Darmstadt) containing 32.6 mmol HCl at ambient temperature. To expose the X5CrNi18−10 (304) steel samples to the generated Cl_2 gas, they were positioned in the opening of the Erlenmeyer flask (Figure S1a) containing the aqueous $KMnO_4$/HCl mixture, which was continuously stirred at room temperature. Surface oxidation was carried out for 50 min (sample group SO50), 60 min (sample group SO60), 95 min (sample group SO95), 142 min (sample group SO142), and 300 min (sample group SO300). After surface oxidation, the samples were rinsed with tap water for 15 min and then with deionized water for an additional 10 min. Each sample group comprised four samples prepared in the same way (Table 1, Figure S1b). Untreated AISI 304 steel cleaned with ethanol, polished with grit 600 SiC sanding paper, and rinsed with deionized water was used as s sample reference.

Table 1. Sample Overview[a]

sample	oxidation	temperature (K)	duration (min)	overpotential (mV)
SO50	Cl_2 gas	293	50	307−335
SO60	Cl_2 gas	293	60	265−276
SO95	Cl_2 gas	293	95	268−286
SO142	Cl_2 gas	293	142	257−282
SO300	Cl_2 gas	293	300	275−285
reference	no oxidation	293	-	370−407

[a]The overpotential was determined at 1.5 mA/cm^2 current density in 0.1 M KOH. Untreated AISI 304 steel was used as reference sample. Each sample was prepared and characterized four times.

Electrochemical Characterization. A three-electrode setup was used for all electrochemical measurements. The AISI 304 steel samples were used as working electrodes, on which surface areas of 1.5−2.1 cm^2 were exposed, while the remaining surface area was protected with insulating Kapton tape. A platinum wire electrode (geometric area 2 × 2 cm) was employed as a counter electrode. Cyclic voltammograms (CVs) were recorded under stirring (180 rpm) using a magnetic stirrer and a stirring bar with a length of 15 mm. The scan rate was set to 20 mV/s, and the step size was set to 2 mV. Chronopotentiometry scans with a duration of 100 000−150 000 s were recorded under stirring as described above. In all measurements, the reference electrode was placed in between the working and counter electrodes. The distances between working electrode and reference electrode as well as the distances between reference electrode and the counter

DOI: 10.1021/acscatal.5b00221
ACS Catal. 2015, 5, 2671−2680

Table 2. Cationic Distribution and Position of the $2p_{3/2}$ Main Lines of Cr, Fe, and Ni of Sample SO60, Sample SO95, and Untreated AISI 304 Steel Derived from the XPS Measurements Presented in Figures 3a−c[a]s

	cationic distribution (at. %)			position of $2p_{3/2}$ line (± 0.25 eV)		
element	Cr	Fe	Ni	Cr	Fe	Ni
sensitivity factor	2.488	2.946	3.702			
sample SO50	29.2%	68.7%	1.6%			
sample SO60	31.4%	63.8%	4.8%	576.5 eV	711.0 eV	855.75 eV
sample SO95	53.3%	43.3%	3.4%			
sample SO300	51.2%	46.5%	2.3%			
reference	16.3%	79.7%	4.0%	576.5 eV	(706.5 eV) 710.1 eV	(852.5 eV) 855.75 eV

[a]Measurements performed before and after carrying out the chronopotentiometry scans (duration: 150 000 s) showed the same value.

electrode were adjusted to 4−5 mm. All electrochemical data were digitally recorded using a Potentiostat Interface 1000 manufactured by Gamry Instruments (Warminster, PA, U.S.A.) connected to a personal computer. Ohmic losses were corrected by subtracting the ohmic voltage drops from the measured potentials using an electrolyte resistance determined by high-frequency alternating current impedance. IR-corrected potentials are denoted as E-IR. The overpotentials of all surface oxidized samples (Table 1) were always derived from steady-state measurements, i.e., from chronopotentiometry plots (duration 100 000 or 150 000 s) in 0.1 M KOH at 1.5 mA/cm^2 current density or in 0.1 M KH_2PO_4/K_2HPO_4 at 0.65 mA/cm^2. The total amount of electrolyte was 70 mL for the measurement of cyclic voltammograms and 350 mL for the measurement of long-time chronopotentiometry plots.

Electrochemical Measurements in Alkaline Medium. All voltages were measured against a reversible hydrogen reference electrode (RHE, HydroFlex, Gaskatel Gesellschaft für Gassysteme durch Katalyse and Elektrochemie mbH, Kassel, Germany). The measurements were performed in a 0.1 M KOH solution (Merck TitriPur, Darmstadt, Germany). For recording CVs, the potential was cyclically varied between 1.0 and 1.7 V vs RHE. CVs of samples SO50−SO300 were recorded directly after treatment with Cl_2 and after 150 000 s of chronopontentiometry at 1.5 mA/cm^2 current density. Stability scans were conducted in the chronopotentiometry mode at a constant current of 3 mA.

Electrochemical Measurements in Neutral Medium. All voltages were measured against a Ag/AgCl electrode (Metrohm, 70794 Filderstadt, Germany) except in long-time chronopotentiometry measurements which were performed using a RHE as reference electrode. For measurements at pH 7, a solution of 0.1 M KH_2PO_4/K_2HPO_4 (VWR, 99% purity) in Millipore water (resistivity >18 MΩ cm) was used. For recording CVs, the potential was cyclically varied between 0.40 and 1.25 V vs Ag/AgCl. Stability scans were conducted in the chronopotentiometry mode at a constant current of 1 mA.

Determination of Nickel, Chromium, and Iron Ions. Concentrations of Ni ions, Cr ions and Fe ions in the electrolytes used for long time chronopotentiometry as well as in the rinsing water used to clean the samples after chlorination were determined as follows.

One hundred milliliters of the electrolyte used for the long time chronopotentiometry (or rinsing water) was added to a 250 mL glass beaker. The solution was neutralized under stirring by adding around 105 mL of 0.05 M H_2SO_4 (Merck TitriPur, Merck, Darmstadt, Germany) until pH 4 was reached. The solution was concentrated by heating up to 95 °C until the total volume reached 40 mL. After cooling down 1 g of $K_2S_2O_8$ (99% purity, VWR, Darmstadt, Germany) was added, and the mixture was again heated to 95 °C for additional 3 min. There was no yellow coloration indicating that $Cr_2O_7^{2-}$ ion was obtained. Detection limit was <2 ppm. Twenty mL of the electrolyte used for the long time chronopotentiometry (or rinsing water) was added to a 100 mL glass beaker (beaker Nr. 1). The solution was neutralized under stirring by adding around 20 mL of 0.1 M HCl (99% purity, VWR, Darmstadt, Germany) until pH 6 was reached. The amount of 10 mL was taken from the solution and filled in a second 100 mL glass beaker (beaker Nr. 2).

The solution of beaker Nr. 2 was concentrated upon heating to 95 °C for 30 min until the volume reached 3 mL, and after cooling, 60 mg of potassium ferrocyanide $K_4[Fe(CN)_6]$ (99% purity, Carl Roth, Karlsruhe, Germany) was added. The mixture formed was shaken for 1 min. Neither a precipitation nor a coloration took place showing that neither Fe^{2+} nor $Fe^{3+}$was present. Detection limit <1 ppm. After 20 min 1 mL of saturated H_2O_2 (30 wt %, VWR, Darmstadt, Germany) was added to the remaining solution (beaker Nr.1), and the solution was concentrated by heating to 95 °C for 30 min until the total volume reached 3 mL. After cooling to room temperature, 1 mL of saturated ammonia (25 wt %, VWR, Darmstadt, Germany) was added (pH 10). No precipitation was formed proving that no iron ions were present. One milliliter of 0.1 M ethanolic disodium bis (dimethylglyoximate) (99% purity, Carl Roth, Karlsruhe, Germany) was added. No red precipitation was formed proving that no nickel ions were present. Detection limit was <1 ppm.

X-ray Photoelectron Spectroscopy (XPS). XPS measurements using a PHI 5600ci Multitechnique spectrometer equipped with a monochromatic Al Kα source (full width at half-maximum = 0.3 eV) were recorded at room temperature before and after the chronopotentiometry scans. The overall resolution of the spectrometer is 1.5% of the pass energy of the analyzer, corresponding to 0.7 eV. The obtained XP spectra were calibrated with measurements of the Au $4f_{7/2}$ level (84.0 eV) of a gold foil. To evaluate the cationic composition of the tested samples, a standard Shirley background was subtracted from all XP spectra. The relative elemental concentrations of Cr, Fe, and Ni were determined using PHI sensitivity factors (see Table 2) included in the PHI Multipak program package.

Scanning Electron Microscopy (SEM). Surface morphologies of surface-oxidized samples were imaged with a scanning electron microscope (SEM) Zeiss Auriga at accelerating voltages of 5 kV. SEM images were acquired with a secondary electron detector. Atomic force microscopy (AFM) measurements were performed in contact mode using a Quesant Instrument Q250 device equipped with NP-S cantilevers with nominal lengths of 200 μm (±5 μm); 0.58 N/m force constant.

DOI: 10.1021/acscatal.5b00221
ACS Catal. 2015, 5, 2671−2680

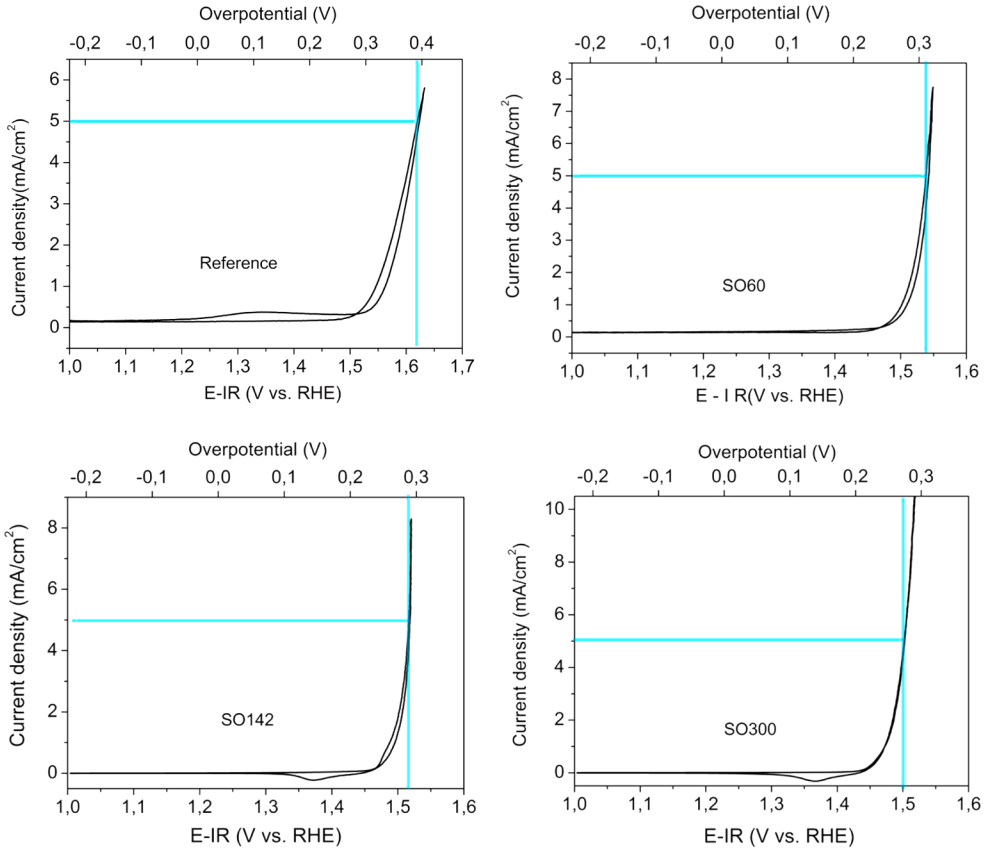

Figure 1. Cyclic voltammograms (CVs) of surface-oxidized samples (SO60, SO142, SO300) and untreated AISI 304 steel (Reference) in 0.1 M KOH recorded after chronopotentiometry for 150 000 s performed in 0.1 M KOH at 1.5 mA/cm^2. Scan rate: 20 mV/s; step size: 2 mV. Extrapolated overpotential at 5 mA/cm^2: 392 mV (Reference), 312 mV (SO60), 292 mV (SO142), 282 mV (SO300).

The AFM images were processed with the free software package Gwydion.

3. RESULTS AND DISCUSSION

Electrochemical Properties of Surface-Oxidized Samples SO50−SO300 at pH 13. Figure 1 displays CVs of samples SO60, SO142, and SO300 recorded after chronopotentiometry performed for 150 000 s in 0.1 M KOH at 1.5 mA/cm^2 and as well a CV of an untreated AISI 304 (Reference sample) recorded in 0.1 M KOH. The CVs of samples SO60, SO142, and SO300 (Figure 1) recorded after chronopotentiometry for 150 000 s are identical to the corresponding CVs recorded directly after surface oxidation. Neither the measurement of CVs nor the long-time chronopontentiometry changed the electrochemical behavior of the surfaces of the oxidized AISI 304 steel samples (Table 2). The CVs of the surface-oxidized AISI 304 steel resemble those of untreated iron or stainless steel in absence of catalytic active Ni sites: There are no significant redox peaks which could be assigned to Ni(II)−Ni(III) and Ni(III)−Ni(II) transitions (Figure 1). Hence, we found no evidence that active Ni sites are on the surfaces of samples SO50−SO300 or on the surface of untreated AISI 304 steel. This finding could be confirmed by XPS experiments performed directly after the surface oxidation as well as after chronopotentiometry for 150 000 s at pH 13; the XP spectra remained unchanged and showed no significant Ni contamination on or close to the surface (Table 2). The sample surfaces are dominated by Fe oxides and Cr oxides. As obvious from the cationic distribution, the sum of the Fe and Cr content on the surface exceeds in all surface-oxidized samples 95% (Table 2). However, surface oxidation with Cl_2 gas led to significant enrichment of Cr species at the sample surfaces (Table 2, Scheme 1). Whereas on the surface of untreated AISI 304 steel a Cr content of 16.3% was detected, the Cr content significantly increased after 60 min Cl_2 treatment to 31.4% (sample SO60). After 95 min exposure to Cl_2, the Cr content of 53.3% already exceeded the Fe content. Further extension of the surface oxidation to up to 300 min did not result in further increase in the Cr content (Table 2). A direct comparison of the CV curves of surface-oxidized samples SO60, SO142, and SO300 with those of the reference sample evidence significant enhancement of the electrocatalytic OER performance associated with surface oxidation with Cl_2 (Figure 1). The onset of the current jump, i.e., the potential at which the current significantly increased, was found to be significantly shifted toward lower potentials in the case of surface-oxidized AISI 304 steel, i.e., the "onset potential" (P_{onset}) seem to correlate with the reciprocal of the chlorination duration (P_{onset} (SO300)< P_{onset} (SO142) < P_{onset} (SO60) < P_{onset} (Reference)). Within the CV curves belonging to untreated AISI 304 steel, the current significantly increased at 1.52 V vs RHE (Figure 1). However, the current initiated by surface-oxidized samples, e.g., sample group SO300, started to increase abruptly already at 1.45 V vs RHE (Figure 1). Due to the pronounced stability of all surface-oxidized samples in alkaline medium, as discussed below, it should be possible to extrapolate overpotentials on the basis of CV measurements. While comparing estimated overpotentials at 5 mA/cm^2, we could (again) obtain

DOI: 10.1021/acscatal.5b00221
ACS Catal. 2015, 5, 2671−2680

Scheme 1. Illustration of the Enrichment of Chromium on the Surface of AISI 304 Steel in the Course of Surface Oxidation by Chlorination[a]

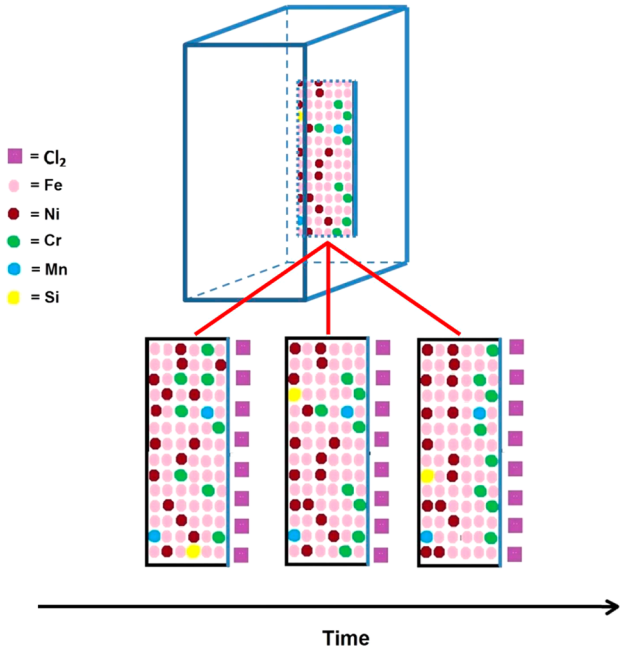

[a]The scheme shows cross sections of the steel specimens representing the situation after different chlorination times.

a clear shift within the sample series Reference, SO60, SO142, and SO300. The CV curves were shifted toward lower potential with increasing duration of the chlorine treatment (Figure 1). The estimated overpotential of untreated AISI 304 is 392 mV at 5 mA/cm^2 (Figure 1). The corresponding value of sample SO60 amounts to ~312 mV at 5 mA/cm^2 (Figure 1) and is somewhat higher than the corresponding overpotentials of sample SO142 (292 mV at 5 mA/cm^2) and sample SO300 (282 mV at 5 mA/cm^2) (Figures 1). This horizontal shift of the CV curve may be rationalized by a change in the chemical nature of the surface during surface oxidation. An increase in the active area caused by the surface oxidation, which could be one possible reason for higher currents at specific potentials, would lead to a vertical shift of the CV curves toward higher current densities. However, AFM investigations suggested that surface roughness rather decreases during chlorination (cf. corresponding AFM images of sample groups SO60 and SO95; Figures S2–S4). Although the surface-oxidized samples show CV curves (Figure 1) resembling those of pure, untreated iron,[36−38] we measured electrocatalytic performances for SO60, SO142, and SO300 that were superior to those of pure iron or iron alloys. Lyons and Doyle reported the activation of iron via cyclic oxidation in alkaline medium and found for the overpotential in 0.1 M NaOH values of ~600 mV at 10 mA/cm^2[34] and of 360 mV in 1 M NaOH at 1 mA/cm^2.[33]

In order to judge the overall electrocatalytic performance, steady-state measurements like chronopotentiometry are more meaningful than CVs. Figure 2 shows long-time chronopotentiometry plots of surface-oxidized samples SO60, SO142, and SO300 as well as the chronopotentiometry plot of untreated AISI 304 steel recorded in 0.1 M KOH at 1.5 mA/cm^2. All surface-oxidized samples were found to be electrocatalysts with excellent stability in alkaline regime, as obvious from the chronopotentiometry plots of samples SO60, SO142,

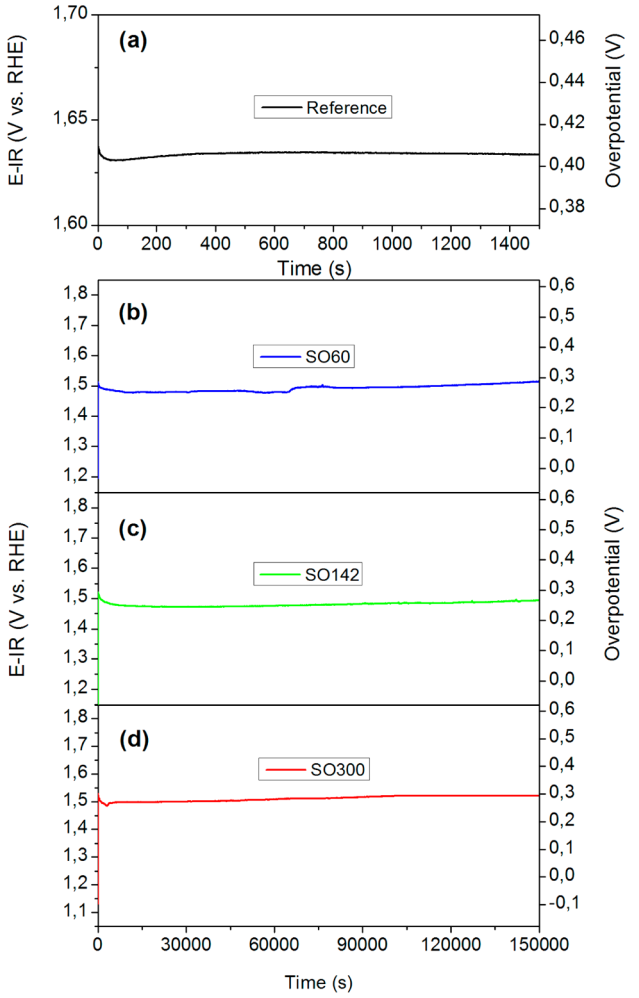

Figure 2. Comparison of the stability of untreated AISI 304 steel (Reference) and surface-oxidized samples SO60, SO142, and SO300 under water-splitting conditions in alkaline medium. (a) Chronopotentiometry plot of untreated AISI 304 steel (Reference) measured in 0.1 M KOH. The average overpotential amounted to 407 mV at 1.5 mA/cm^2, the start potential (t = 90 s) was 1.631 V vs RHE, the end potential (t = 1500 s) was 1.63 V vs RHE. (b) Long-term chronopotentiometry plot of sample SO60 measured in 0.1 M KOH. The average overpotential amounted to 272 mV at 1.5 mA/cm^2, the start potential (t = 90 s) was 1.5 V vs RHE, the end potential (t = 150 000 s) was 1.515 V vs RHE. (c) Long-term chronopotentiometry plot of sample SO142 measured in 0.1 M KOH. The average overpotential amounted to 265 mV at 1.5 mA/cm^2, the start potential (t = 90 s) to 1.515 V vs RHE, and the end potential (t = 150000 s) to 1.495 V vs RHE. (d) Long-term chronopotentiometry plot of sample SO300 measured in 0.1 M KOH. The average overpotential amounted to 282 mV at 1.5 mA/cm^2, the start potential (t = 90 s) to 1.52 V vs RHE, and the end potential (t = 150 000 s) to 1.523 V vs RHE.

and SO300 (Figure 2). This finding is not self-evident because Fe_2O_3 has a relatively high solubility in alkaline aqueous solutions causing a transfer of Fe from the anode to the cathode under operating conditions.[39]

In the case of the untreated AISI 304 steel, an average potential of 1.635 V is required to guarantee a total current of 3 mA (current density 1.5 mA/cm^2; Figure 2a). The overpotential could be reduced by around 135 mV by surface-oxidation for 60 min (sample group SO60; Figure 2b). Even after chronopotentiometry performed for 150 000 s at 1.5 mA/cm^2, the catalytic performance did not deteriorate; the potential

DOI: 10.1021/acscatal.5b00221
ACS Catal. 2015, 5, 2671−2680

required to guarantee 3 mA total current was only shifted by 15 mV (Figure 2b), showing an average overpotential of 272 mV. These observations confirm the excellent long-term stability of sample SO60. Samples obtained by longer surface oxidation proved to be even more stable than sample SO60. Especially samples surface-oxidized for more than 1 h, e. g., for 95 min (sample SO95), 142 min (sample SO142), or for 300 min (sample SO300), proved to be water-splitting electrocatalysts exhibiting excellent stability in alkaline media even after tens of hours of operation in 0.1 M KOH at 1.5 mA/cm^2 (Figures S5, 2c,d). Four hours after the start of the chronopotentiometry, the overpotential of samples SO95, SO142, and SO300 determined in 0.1 M KOH at 1.5 mA/cm^2 was below 270 mV and remained in this range (Figures S5,2c,d). The overpotentials of the surface-oxidized samples derived from these steady-state measurements do not significantly differ; independent of the duration of the surface oxidation they lie in the range from 265 mV to 285 mV (Table 1). Sample SO60, which was exposed to chlorine for 1 h at an average overpotential of 272 mV in 0.1 M KOH at 1.5 mA/cm^2 represented the best compromise regarding overall OER activity and electrocatalytic stability, taking into account the significantly reduced exposure time in comparison with SO142 and SO300. Samples surface-oxidized for less than 60 min (sample SO50) showed higher overpotentials with values ranging from 307 mV to 335 mV at 1.5 mA/cm^2 (cf. Table 1, Figure S6).

In the course of these electrochemical measurements, gas bubbles formed on all surface-oxidized steel samples. We clearly assign the detected current to the OER and not to possibly occurring oxidation of metallic species still existing on the surface after the surface oxidation by Cl_2 gas. This assignment could also be confirmed by XPS measurements (Figure 3) showing no nonoxidized metallic species (Fe, Cr, Ni) on the surface of the surface-oxidized AISI 304 samples, whereas untreated AISI 304 steel shows some small amounts of Fe^0. Figure 3 displays high-resolution Cr 2p, Fe 2p, and Ni 2p spectra of sample SO60 representative of all surface-oxidized samples as well as high-resolution Cr 2p, Fe 2p, and Ni 2p spectra of untreated AISI 304 steel. The 2 $p_{3/2}$ positions of several reference compounds are indicated by gray vertical bars.[40−42,47,48] The binding energies apparent in Figure 3a suggest that no metallic Cr or Cr(VI) oxide is present neither in sample SO60 nor in untreated AISI 304 steel.

Most likely, Cr is present in form of Cr^{III}, either as Cr_2O_3, as Cr(III)hydroxide, or as admixture of both species (Figure 3a). Evaluation of the Fe 2p3/2 binding energies revealed that iron in the form of FeOOH species clearly dominates at the surfaces of the surface-oxidized samples. XPS spectra recorded prior to and after chronopotentiometry for 150 000 s in 0.1 M KOH at 1.5 mA/cm^2 were identical. This outcome rules out that ongoing surface oxidation of the oxidized surfaces occurred during chropotentiometry. The electrolytes used for the long-term chronopotentiometry scans did not contain detectable amounts of Fe, Ni, or Cr ions as could be proven by an analysis of the 0.1 M KOH after usage for chronopotentiometry (see Experimental Details). In addition, the mass of the samples remained unchanged during the electrochemical measurements (Table S1). We determined the mass of the surface-oxidized samples prior and after the long time chronopotentiometry measurements and drying for 60 min at 80 °C under air (Table S1). In principle, it is conceivable that AISI 304 steel forms metal chlorides upon chlorination and dissociation leads to transfer of chloride ions in the electrolyte solutions. During the CVs or the chronopotentiometry mesurements, a Cl_2 evolution reaction would then be possible. However, no chloride ions and no Fe, Ni, or Cr ions could be found in the rinsing water (Cl^- detection with $AgNO_3$ solution showed no precipitation) after cleaning the specimen.

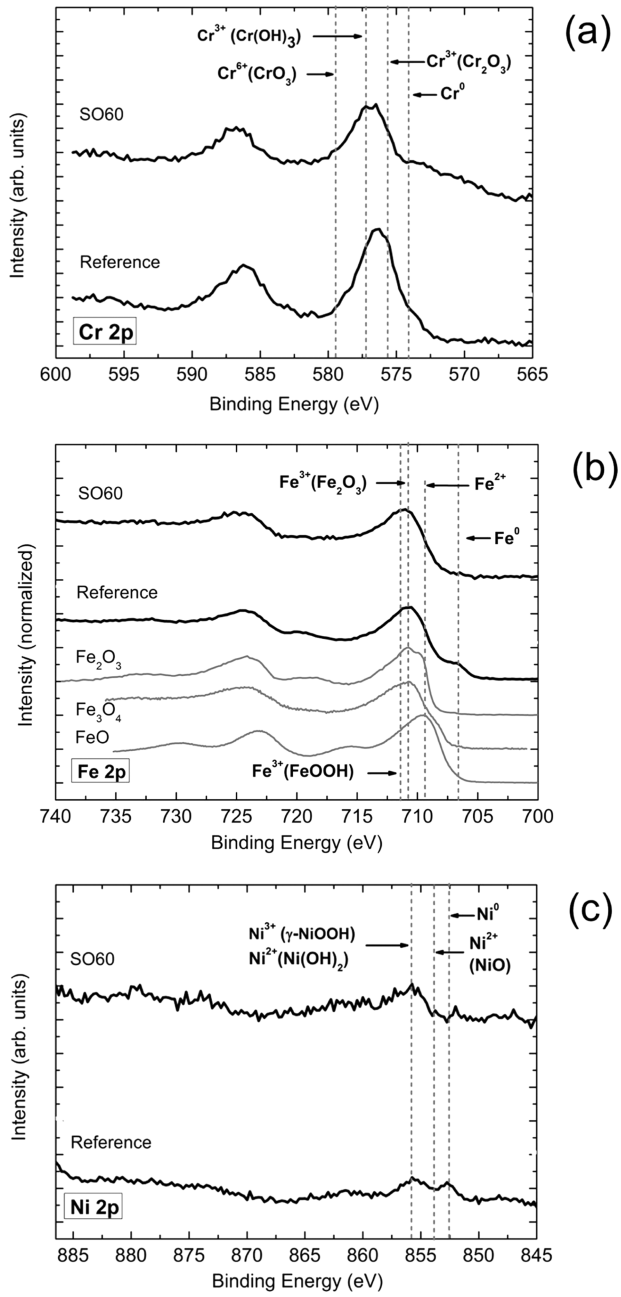

Figure 3. XPS characterization of sample SO60 and untreated AISI 304 steel (Reference). (a) Cr 2p core levels. Binding energies of metallic Cr as well as CrO_3, $Cr(OH)_3$, and Cr_2O_3 Reference compounds are indicated by vertical lines as a guide to the eyes.[41] (b) Fe 2p core levels. Binding energies of FeO, Fe_2O_3, and Fe_3O_4 reference compounds are indicated by vertical lines as a guide to the eyes.[40,42] (c) Ni 2p core levels. Binding energies of metallic Ni, as well as γ−NiOOH, $Ni(OH)_2$ and NiO reference compounds are indicated by vertical lines as a guide to the eyes.[41,47,48]

Little efforts have been focused on the evaluation of the electrocatalytic OER properties of steel. To the best of our knowledge, Chatenet et al. published the highest OER activity

DOI: 10.1021/acscatal.5b00221
ACS Catal. 2015, 5, 2671−2680

for steel (330 mV overpotential at 10 mA/cm^2 in 1 M KOH). In terms of catalytic activity, our best samples (SO60, SO142, SO300) are almost at the level of the samples with the highest ever measured activity values: $NiCo_2O_4$–graphene hybrid,[43] nanochrystalline Ni_3S_2 supported by Ni metal,[27] CuFe-$(MoO_4)_3$,[28] $NiCo_2O_4$ aerogel,[44] $Ni_xFe_y(OH)_2$,[45] and $Ni_xFe_yO_z$ nanoparticles supported on glassy carbon.[46] Yet, it is not possible to unambiguously evidence that the enrichment of Cr species at the surface (Scheme 1) of the surface-oxidized AISI 304 samples occurs according to a specific mechanism. In addition the outcome of the findings described so far, do not prove beyond reasonable doubt that the formed Fe–Cr oxide layer on the surface of our oxidized samples is responsible for their superior electrocatalytic properties in comparison with untreated AISI304 steel. A dissolution-based mechanism or a dissolution–precipitation process is difficult to imagine taking into account that the enrichment occurs at ambient conditions in a gas atmosphere. On the other hand, driving forces for diffusion-based mechanisms, such as electromigration, are absent under these conditions.

In order to clarify if the existence of a Fe–Cr oxide layer on the periphery of the stainless steel caused the enhancement of the electrocatalytic properties, we performed an additional experiment. We intended to simulate an alloy consisting of 32 wt % Cr and 68 wt % Fe (which is commercially not accessible) via a very easy approach by pressing a chromium disk into pure iron (Figure S7). Afterward the sample was surface oxidized by Cl_2 gas for 5 h under ambient conditions to achieve Fe/Cr-oxide on the surface. For the electrochemical measurements, a specific area was defined by using Kapton tape in a way that around 32% of the area is covered by chromium species and around 68% of the area is covered by Fe species. This specimen (Chlorinated Cr/Fe composite) should act as a model for sample SO60 on which surface the cationic distribution was found to be 31% Cr and 64% Fe. Indeed, the electrochemical behavior of chlorinated Cr/Fe composite is superior to that of chlorinated iron and comparable to that of sample SO60 (Figure S8), which should be considered as a hint that the existence of Fe–Cr oxide layer on the periphery of our surface oxidized AISI 304 stainless steel indeed caused the enhancement of the electrocatalytic oxygen evolution performance.

The role Cr plays in enhancing the Fe-based OER properties is, up to now, not fully understood. We speculate that during the chlorination of the AISI 304 steel, the presence of Cr enables a perfect homogenization of the active Fe spots, as required for superior catalytic properties. Very likely a homogenization of active Ni spots by Fe incorporation plays a major role for the dramatically increased activity of the electrocatalytic initiated oxygen evolution of electrodeposited Ni/Fe oxyhydroxide thin films.[45]

Electrochemical Properties of Surface-Oxidized Samples SO60–SO300 at pH 7. The electrochemical properties of untreated AISI 304 steel as well as of samples SO60, SO142, and SO300 in pH 7 buffer solution are summarized in Figure 4. The CV curves of untreated AISI 304 steel recorded in neutral regime were found to be shifted to lower potential upon surface oxidation with chlorine as well. A direct comparison of the CV curves derived from the surface-oxidized sample SO60 and untreated AISI 304 steel reveals significant enhancement of the electrocatalytic OER performance of sample SO60 as compared to untreated AISI 304 steel (Figure 4a,b). Even at a potential of 1.2 V vs Ag/AgCl, which corresponds to an overpotential of 582.7 mV, untreated AISI 304 steel initiates only very weak oxygen evolution at a current density of ~0.2 mA/cm^2 (Figure 4a). A more than 10 times higher current density could be detected for surface-oxidized sample SO60 at the same

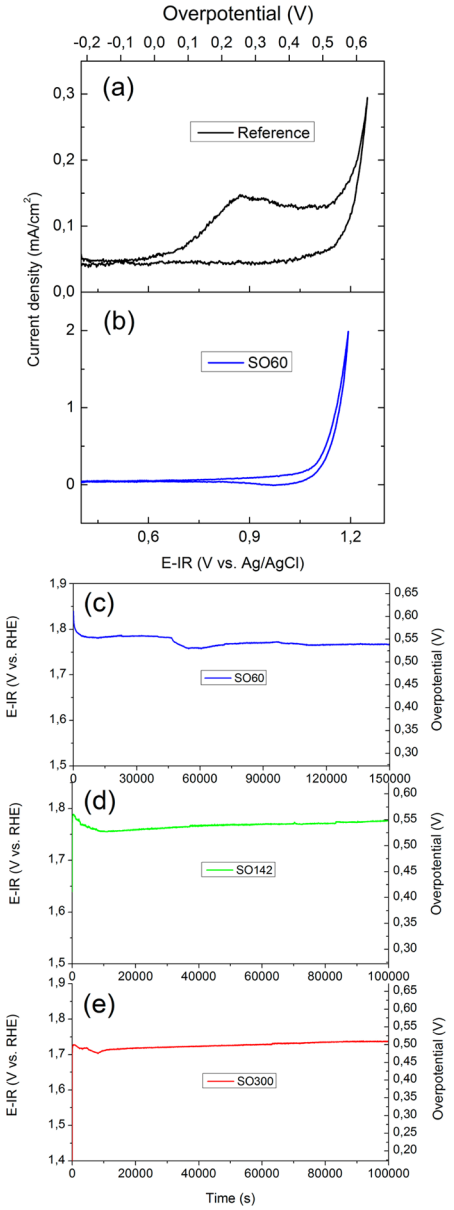

Figure 4. Electrochemical behavior of untreated AISI 304 steel and surface-oxidized samples SO60, SO142, and SO300 in the neutral regime. (a) Cyclic voltammogram of untreated AISI 304 steel recorded at pH 7 in 0.1 molar KH_2PO_4/K_2HPO_4 solution. The scan rate was 20 mV/s, and the step size was 2 mV. (b) Cyclic voltammogram of sample SO60 recorded at pH 7 in 0.1 molar KH_2PO_4/K_2HPO_4 solution. The scan rate was 20 mV/s, and the step size was 2 mV. (c) Long-term chronopotentiometry plot of SO60 measured in 0.1 M KH_2PO_4/K_2HPO_4. The average overpotential was 552 mV at 0.65 mA/cm^2, the start potential (t = 90 s) amounted to 1.818 V vs RHE, and the end potential (t = 150 000 s) was 1.767 V vs RHE. (d) Long-term chronopotentiometry plot of sample SO142 measured in 0.1 M KH_2PO_4/K_2KHPO_4. The average overpotential amounted to 542 mV at 0.65 mA/cm^2, the start potential (t = 90 s) to 1.78 V vs RHE, and the end potential (t = 100 000 s) to 1.78 V vs. RHE. (e) Long-term chronopotentiometry plot of sample SO300 measured in 0.1 M KH_2PO_4/K_2KHPO_4. The average overpotential amounted to 502 mV at 0.65 mA/cm$_2$, the start potential (t = 90 s) to 1.726 V vs RHE, and the end potential (t = 100 000 s) to 1.736 V vs RHE.

DOI: 10.1021/acscatal.5b00221
ACS Catal. 2015, 5, 2671–2680

potential (Figure 4b). At pH 7, oxygen evolution properties of untreated AISI 304 steel were found to be so poor that we could not record reasonable chronopontentiometry scans. It was not possible to detect a reasonable current at an acceptable overpotential, as obvious from the corresponding CV (Figure 4a).

The electrocatalysts obtained by chlorination of AISI 304 steel proved to be very stable also in the neutral regime (Figure 4c,d,e). In the case of sample SO60, the potential required to guarantee 0.65 mA/cm^2 was found to be even reduced within 150 000 s of chronopontentiometry scan from 1.818 to 1.767 V. In the case of sample SO300, the corresponding potential was increased by only 10 mV from 1.726 to 1.736 V. Therefore, the water-splitting characteristics of all surface-oxidized AISI 304 steel samples did not deteriorate even after tens of hours chronopotentiometry at pH 7 in phosphate buffer solution (Figure 4c,d,e). However, in neutral media, the surface-oxidized AISI 304 steel samples seem to be less efficient for the electrocatalytic initiated oxygen evolution as compared to their behavior in alkaline medium (Figure 4c,d,e); in neutral medium, the overpotentials lie between 500 and 550 mV at 0.65 mA/cm^2. The three chronopotentiometry plots of the surface-oxidized samples SO60, SO142, and SO300 (Figure 4c−e) reveal a clear trend with respect to the overpotential measured in 0.1 M KH_2PO_4/K_2HPO_4 buffer solution at 0.65 mA/cm^2 current density. The overpotential decreased with increasing duration of the surface oxidation. Whereas for sample SO60 an average overpotential of 552 mV was found, the corresponding value of sample SO142 was 542 mV and finally an overpotential of 502 mV was measured in the case of sample SO300 at pH7 and at 0.65 mA/cm^2. However, taking into account the cheapness of AISI 304 steel, the enormous stability of surface-oxidized AISI 304 steel under water-splitting conditions and the facile surface oxidation procedure, we consider at least sample SO300 as an interesting water-splitting electrocatalyst for water cleavage at acceptable overpotential (500 mV at 0.65 mA/cm^2) in neutral medium. This result is interesting and surprising because metal oxides have commonly been considered as instable as oxygen-evolution electrocatalysts in neutral or acidic regime. Only a few exceptions can be found in the literature. Surendranath and Nocera found for cobalt-based catalysts at pH 7 overpotential values of around 0.36−0.4 V at 1 mA/cm^2.[49]

It has remained unclear why the OER at metal-oxide surfaces obviously benefits from high pH values. However, some possible reasons for this outcome can be named. Metal oxides are easily regenerated after oxygen molecule release by coordination of two hydroxide ions followed by proton loss. Both steps are likely to occur because of the high OH^- concentration in the alkaline regime. For the hypothetical release of molecular oxygen in a direct manner, close proximity of two catalytically active oxide based sites as well as easy oxygen-to-metal charge transfer would be advantageous. As there is some time required for the whole sequence of steps, the process is not diffusion-controlled. Nevertheless, there must be high electronic conductivity between the metal oxide catalytic sites and the bulk of the metal to allow high current densities with no or only little ohmic drop. This scenario is especially expected in the case of smooth surfaces. As can be taken from SEM images as well as AFM images, the surface smoothness of the chlorine-treated AISI 304 was preserved (Figures 5, S2−S4).

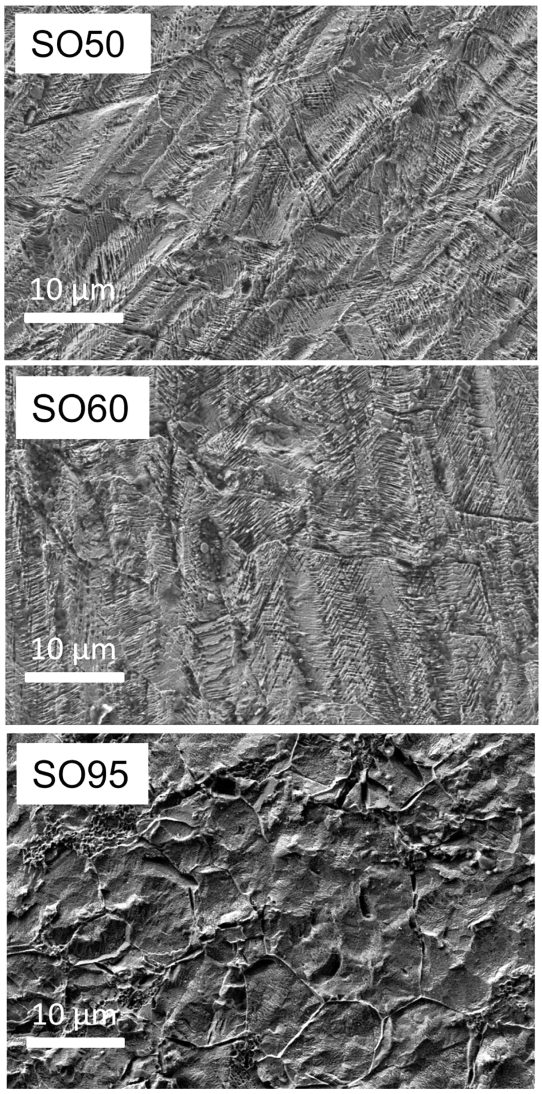

Figure 5. SEM images of selected surface-oxidized AISI 304 steel samples showing the surface topography.

4. CONCLUSIONS

The electrochemically initiated oxygen evolution (OER) plays, besides the corresponding hydrogen evolution reaction (HER), a key role in environmentally friendly energy production. Hoare showed that the potential at which oxygen can be produced on the surface of metal electrodes used as oxygen evolution electrocatalysts is related to the metal/metal oxide couple.[18] Ideal metal/metal oxide couples should exhibit a potential lower than or similar to the reversible H_2O/O_2 potential. Metal/metal oxide couples interesting for the OER based on Fe−Ni-containing species can be found in stainless steel grades such as AISI 304. Such commodity steels consisting of earth-abundant elements are cheap and can be produced at high quantities but show poor performance as OER electrocatalysts. We have shown that simple surface oxidation by exposure to gaseous chlorine converts the stainless steel AISI 304 into a highly active OER electrocatalyst under alkaline and neutral conditions. Surface-oxidized AISI 304 steel showed a stable current density of 1.5 mA/cm^2 at ∼260 mV overpotential in 0.1 M KOH. The extrapolated value of the overpotential derived from the CV may be as low as 300 mV at 5 mA/cm^2 in 0.1 M KOH. Even after tens of hours chronopotentiometry at 1.5

DOI: 10.1021/acscatal.5b00221
ACS Catal. 2015, 5, 2671−2680

mA/cm^2 and at pH 13, the electrocatalytic performance of the surface-oxidized AISI 304 steel did not deteriorate. The potential required to guarantee a fixed current density remained in alkaline regime on the level of the start value as can be taken from the long time (150 000 s chronopotentiometry plots). XPS analysis revealed that thin films of Fe oxides and Cr oxides firmly attached to the steel substrates had been formed on the surface-oxidized AISI 304 steel specimens, and Cr enrichment had occurred at their surfaces. Depending on the process parameters applied during surface oxidation, the purity of the Fe oxide and Cr oxide lies between 95% and 98%. Although oxide layers formed on mild steel by exposure to gaseous Cl_2 have thicknesses in the micrometer range, we estimate the thickness of the oxide layers formed on AISI 304 steel to be smaller than 5 nm. All surface-oxidized AISI 304 steel samples showed excellent catalytic stability in the neutral regime, as obvious from the stable OER currents even after tens of hours operation time. However, the potential necessary to guarantee a stable OER current in KH_2PO_4/K_2KHPO_4 solution at pH 7 was significantly higher (between 500 and 550 mV at 0.65 mA/cm^2 in 0.1 M KH_2PO_4/K_2KHPO_4) than at pH 13 (between 257 and 335 mV at 1.5 mA/cm^2 in 0.1 M KOH). Nevertheless, we consider at least sample SO300 as an interesting water-splitting electrocatalyst for cleavage of water at an acceptable overpotential (500 mV at 0.65 mA/cm^2) in neutral regimes that is cheap, easy to handle, and outstandingly stable under water-splitting conditions. Surface-oxidized stainless steel is a promising commodity electrode for electrocatalyzed oxygen evolution in both alkaline and neutral regimes and is cheap, available at large quantities, stable, nontoxic, and characterized by excellent electrocatalytic properties.

■ ASSOCIATED CONTENT

Supporting Information

The following file is available free of charge on the ACS Publications website at DOI: 10.1021/acscatal.5b00221.

An image of the chlorination experiment, additional chronopotentiometry scans as well as AFM images of selected steel samples, and a table showing the cationic distribution and position of the $2p_{3/2}$ main lines of Cr, Fe, and Ni of samples (PDF)

■ AUTHOR INFORMATION

Corresponding Author

*E-mail: helmut.schaefer@uos.de.

Notes

The authors declare no competing financial interest.

■ REFERENCES

(1) Walter, M. G.; Warren, E. L.; McKone, J. R.; Boettcher, S. W.; Mi, Q.; Santori, E. A.; Lewis, N. S. *Chem. Rev.* **2010**, *110*, 6446−6473.
(2) Cook, T. R.; Dogutan, D. K.; Reece, S. Y.; Surendranath, Y.; Teets, T. S.; Nocera, D. G. *Chem. Rev.* **2010**, *110*, 6474−6502.
(3) Bard, A. J.; Fox, M. A. *Acc. Chem. Res.* **1995**, *28*, 141−145.
(4) Lyons, M. E. G.; Doyle, R. L.; Brandon, M. P. *Phys. Chem. Chem. Phys.* **2011**, *13*, 21530−21551.
(5) Koper, M. T. M. *J. Electroanal. Chem.* **2011**, *660*, 254−260.
(6) Kanan, M. W.; Nocera, D. G. *Science* **2008**, *321*, 1072−1075.
(7) Gorlin, Y.; Jaramillo, T. F. *J. Electrochem. Soc.* **2012**, *159*, H782−H786.
(8) Lee, Y.; Suntivich, J.; May, K. J.; Perry, E. E.; Shao-Horn, Y. *J. Phys. Chem. Lett.* **2012**, *3*, 399−404.
(9) Gorlin, Y.; Jaramillo, T. F. *J. Am. Chem. Soc.* **2010**, *132*, 13612−13614.
(10) Trasatti, S. *Electrochim. Acta* **1984**, *29*, 1503−1512.
(11) Trasatti, S. *Electrochim. Acta* **1987**, *32*, 369−382.
(12) Trasatti, S. *Electrochim. Acta* **2000**, *45*, 2377−2385.
(13) Petrykin, V.; Macounova, K.; Shlyakhtin, O. A.; Krtil, P. *Angew. Chem., Int. Ed.* **2010**, *49*, 4813−4815.
(14) Nakagawa, T.; Beasley, C. A.; Murray, R. W. *J. Phys. Chem. C* **2009**, *113*, 12958−12961.
(15) Zhao, Y.; Hernandez-Pagan, E. A.; Vargas-Barbosa, N. M.; Dysart, J. L.; Mallouk, T. E. *J. Phys. Chem. Lett.* **2011**, *2*, 402−406.
(16) Lyons, M. E. G.; Brandon, M. P. *J. Electroanal. Chem.* **2010**, *641*, 119−130.
(17) Lyons, M. E. G.; Floquet, S. *Phys. Chem. Chem. Phys.* **2011**, *13*, 5314−5335.
(18) Hoare, J. P. In *Advances in Electrochemistry and Electrochemical Engineering*; Delahay, P.; Tobias, C. W.; Interscience, New York, 1966, Vol. *6*, p 201 -288.
(19) Tseung, A. C. C.; Jasem, S. *Electrochim. Acta* **1977**, *22*, 31−34.
(20) El-Deab, M. S.; Awad, M. I.; Mohammad, A. M.; Ohsaka, T. *Electrochem. Commun.* **2007**, *9*, 2082−2087.
(21) Jiao, F.; Frei, H. *Chem. Commun.* **2010**, *46*, 2920−2922.
(22) Najafpour, M. M. *Dalton Trans.* **2011**, *40*, 3805−3807.
(23) Zhou, F.; Izgorodin, A.; Hocking, R. K.; Spiccia, L.; MacFarlane, D. R. *Adv. Energy Mater.* **2012**, *2*, 1013−1021.
(24) Davidson, C. R.; Kissel, K.; Srinivasan, S. *J. Electroanal. Chem. Interfacial Electrochem.* **1982**, *132*, 129−135.
(25) Bockris, J. O.; Otagawa, T. *J. Electrochem. Soc.* **1984**, *131*, 290−302.
(26) Suntivich, J.; May, K. J.; Gasteiger, H. A.; Goodenough, J. B.; S.-Horn, Y. *Science* **2011**, *334*, 1383−1385.
(27) Zhou, W.; Wu, X.-J.; Cao, X.; Huang, X.; Tan, C.; Tian, J.; Liu, H.; Wang, J.; Zhang, H. *Energy Environ. Sci.* **2013**, *6*, 2921−2924.
(28) Prasad Srirapu, V. K.; Shekhar Sharma, C.; Awasthi, R.; Nath Singh, R.; Kumar Sinha, A. S. *Phys. Chem. Chem. Phys.* **2014**, 7385−7393.
(29) Sato, N.; Okamoto, G. *Electrochim. Acta* **1965**, *10*, 495−502.
(30) Miles, M. H.; Kissel, G.; Lu, P. W. T.; Srinivasan, S. *J. Electrochem. Soc.* **1976**, *123*, 332−336.
(31) Corrigan, D. A. *J. Electrochem. Soc.* **1987**, *134*, 377−384.
(32) Corrigan, D. A.; Bendert, R. M. *J. Electrochem. Soc.* **1988**, *135*, C156−C156.
(33) Lyons, M. E. G.; Doyle, R. E. *Int. J. Electrochem. Sci.* **2011**, *6*, 5710−5730.
(34) Lyons, M. E. G.; Doyle, R. L. *Int. J. Electrochem. Sci.* **2012**, *7*, 9488−9501.
(35) Moureaux, F.; Stevens, P.; Toussaint, G.; Chatenet, M. *J. Power Sources* **2013**, *229*, 123−132.
(36) Lian, K.; Thorpe, S. J.; Kirk, D. W. *Electrochim. Acta* **1992**, *37*, 169−175.
(37) Kessler, T.; Triaca, W. E.; Arvia, A. J. *J. Appl. Electrochem.* **1994**, *24*, 310−315.
(38) Kuhn, A. T.; Wakeman, D.; El Roubi, E. Y.; Collins, G. E. S. *Electrochim. Acta* **1983**, *28*, 515−527.
(39) Wendt, H.; Rausch, S.; Borucinski, T. *Adv. Catal.* **1994**, *40*, 87−176.
(40) Grosvenor, A. P.; Kobe, B. A.; Biesinger, M. C.; McIntrye, N. S. *Surf. Interface Anal.* **2004**, *36*, 1564−1574.
(41) Biesinger, M. C.; Payne, B. P.; Grosvenor, A. P.; Lau, L.W. M.; Gerson, A. R.; Smart, R. St. C. *Appl. Surf. Sci.* **2011**, *257*, 2717−2730.
(42) Klewe, C.; Meinert, M.; Boehnke, A.; Kuepper, K.; Arenholz, E.; Gupta, A.; Schmalhorst, J. M.; Kuschel, T.; Reiss, G. *J. Appl. Phys.* **2014**, *115* (123903), 1−7.
(43) Chen, S.; Qiao, S.-Z. *ACS Nano* **2013**, *7*, 10190−10196.
(44) Chien, H.-C.; Cheng, W.-Y.; Wang, Y.-H.; Wie, T.-Y.; Lu, S.-Y. *J. Mater. Chem.* **2011**, *21*, 18180−18182.
(45) Trotochaud, L.; Young, S. L.; Rannes, J. K.; Boettcher, S. W. *J. Am. Chem. Soc.* **2014**, *136*, 6744−6753.
(46) Qiu, Y.; Xin, L.; Li, W. *Langmuir* **2014**, *30*, 7893−7901.

DOI: 10.1021/acscatal.5b00221
ACS Catal. 2015, 5, 2671−2680

(47) Uhlenbrok, S.; Scharfschwerdt, C.; Neumann, M.; Illing, G.; Freund, H.-J. *J. Phys.: Condens. Matter* **1992**, *4*, 7973−7978.
(48) Biesinger, M. C.; Lau, L. W. M.; Gerson, A. R.; Smart, R. S. C. *Phys. Chem. Chem. Phys.* **2012**, *14*, 2434−2442.
(49) Surendranath, Y.; Dinca, M.; Nocera, D. G. *J. Am. Chem. Soc.* **2009**, *131*, 2615−2620.

DOI: 10.1021/acscatal.5b00221
ACS Catal. 2015, 5, 2671−2680